Editors' Suggestion

Chiral Ising Gross-Neveu Criticality of a Single Dirac Cone: A Quantum Monte Carlo Study

S. Mojtaba Tabatabaei,[1,†] Amir-Reza Negari,[1,†] Joseph Maciejko,[2] and Abolhassan Vaezi[1,*]
[1]Department of Physics, Sharif University of Technology, Tehran 14588-89694, Iran
[2]Department of Physics & Theoretical Physics Institute (TPI), University of Alberta, Edmonton, Alberta T6G 2E1, Canada

(Received 22 December 2021; accepted 4 May 2022; published 3 June 2022)

We perform large-scale quantum Monte Carlo simulations of SLAC fermions on a two-dimensional square lattice at half filling with a single Dirac cone with $N = 2$ spinor components and repulsive on-site interactions. Despite the presence of a sign problem, we accurately identify the critical interaction strength $U_c = 7.28 \pm 0.02$ in units of the hopping amplitude, for a continuous quantum phase transition between a paramagnetic Dirac semimetal and a ferromagnetic insulator. Using finite-size scaling, we extract the critical exponents for the corresponding $N = 2$ chiral Ising Gross-Neveu universality class: the inverse correlation length exponent $\nu^{-1} = 1.19 \pm 0.03$, the order parameter anomalous dimension $\eta_\phi = 0.31 \pm 0.01$, and the fermion anomalous dimension $\eta_\psi = 0.136 \pm 0.005$.

DOI: 10.1103/PhysRevLett.128.225701

Introduction.—Massless Dirac fermions have been identified as the relevant low-energy quasiparticles in various condensed matter systems including graphene, topological insulators, d-wave superconductors, Weyl semimetals, and ultracold fermions in optical lattices [1–7]. Nonetheless, strong interactions can generate a finite mass for the Dirac fermions and spontaneously break some of the symmetries of the model. The quantum phase transitions at which this occurs are typically described by the Gross-Neveu (GN) university classes [8]. In particular, a single Dirac cone in $(2 + 1)D$ subject to on-site repulsive interactions—such as can be found on the surface of a correlated topological insulator—can develop an Ising-type ferromagnetic (FM) order, which generates a $\mathbb{Z}_2$ symmetry-breaking FM mass gap [9,10]. For a chemical potential at the Dirac point, the quantum critical point (QCP) of the resulting transition from semimetal (SM) to insulator is believed to belong to the chiral Ising GN universality class [11–16] with $N = 2$ Dirac spinor components.

Useful insights for the $N = 2$ chiral Ising GN universality class have been obtained from several approaches including the conformal bootstrap, the functional renormalization group (FRG), and analytical field theory methods such as large-N and ϵ expansions. However, these methods so far yield inconsistent results. For example, while the conformal bootstrap [17] predicts $\nu^{-1} = 0.86$, FRG [18] and the ϵ expansion [16] predict $\nu^{-1} = 1.229$ and $\nu^{-1} = 1.276$, respectively. (For other critical exponents, see Table I.) These significant discrepancies demand a resolution from numerically exact quantum Monte Carlo (QMC) simulations which have been unavailable thus far. The lack of QMC studies of this problem originates in part from fermion-doubling theorems which state that a local lattice model cannot realize a single symmetry-protected Dirac cone [19]. Indeed, all previous QMC studies of chiral Ising GN criticality have utilized local lattice models and thus could only access even numbers of Dirac cones, e.g., $N = 4$ [20–23] and $N = 8$ [24–28].

In this Letter, we instead use a nonlocal lattice realization of a single Dirac fermion with $N = 2$ spinor components, known as the SLAC fermion [29–31], subject to an on-site Hubbard repulsion. By employing a state-of-the-art auxiliary-field QMC algorithm, we identify and investigate its FM QCP for the first time [32]. The model is not entirely sign-problem free, but the sign problem is benign at the QCP (Fig. 1) [36]. In this work, we have taken up to several billion measurements to keep the statistical error below

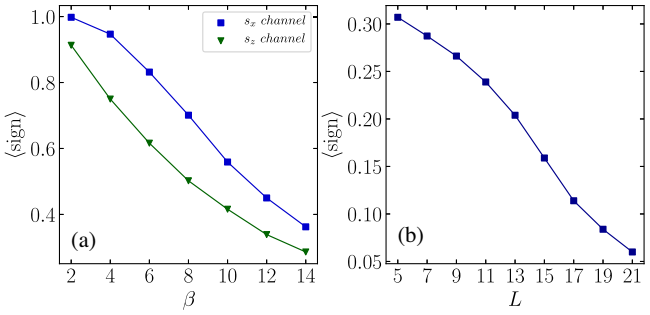

FIG. 1. Behavior of the sign problem in PQMC with $g_{\mathrm{GW}} = 0.17U$ close to the QCP ($U = 7.275$). (a) Decoupling the Hubbard interaction in the s_x channel enhances the average sign compared to the usual s_z channel (here $\beta \equiv 2\Theta$). (b) Average sign of PQMC at $2\Theta = 14$ ($\beta_{\mathrm{eff}} \approx 25 \pm 1$) and $U = 7.275$ as a function of linear system size L.

 © 2022 American Physical Society

TABLE I. Our QMC evaluation of the critical exponents for the $N = 2$ chiral Ising GN universality class, compared with previous estimates.

	ν^{-1}	η_ϕ	η_ψ
This work (QMC)	1.19 ± 0.03	0.31 ± 0.01	0.136 ± 0.005
Conformal bootstrap [17]	0.86	0.320	0.134
FRG [18]	1.229	0.372	0.131
ϵ expansion [16]	1.276	0.2934	0.1400

0.2% [37]. This approach allows us to circumvent the sign problem and accurately extract the critical exponents of the $N = 2$ chiral Ising GN universality class (Table I), our main result.

Model.—We consider an $L \times L$ square lattice with unit lattice constant having a single linearly dispersing Dirac cone in its first Brillouin zone. The free Hamiltonian in momentum space is given by

$$H_0 = \sum_{\mathbf{p}} \Psi_{\mathbf{p}}^\dagger (p_x \sigma_x + p_y \sigma_y) \Psi_{\mathbf{p}}, \tag{1}$$

with $\Psi_{\mathbf{p}}^\dagger = (c_{\mathbf{p}\uparrow}^\dagger, c_{\mathbf{p}\downarrow}^\dagger)$ where $c_{\mathbf{p}\sigma}^{(\dagger)}$ is the electron annihilation (creation) operator with momentum $\mathbf{p} = (p_x, p_y)$ and spin σ, and σ_α, $\alpha = x, y, z$ are the Pauli matrices operating on the spin degree of freedom. We extract the real-space representation of the above Hamiltonian by performing a Fourier transformation, which yields

$$H_0 = \sum_{\mathbf{i}} \sum_{\mathbf{R}} (t_{\mathbf{R}} c_{\mathbf{i}\uparrow}^\dagger c_{\mathbf{i}+\mathbf{R}\downarrow} + \text{H.c.}), \tag{2}$$

where $c_{\mathbf{i}\sigma}^{(\dagger)}$ is the electron annihilation (creation) operator on site $\mathbf{i}$ with spin σ, and $t_{\mathbf{R}}$ denotes the electron hopping amplitude between site $\mathbf{i}$ and $\mathbf{i} + \mathbf{R}$. Here, $\mathbf{R} = (R_x, R_y)$ enumerates all neighbors of site $\mathbf{i}$ along the x and y directions. The explicit form of $t_{\mathbf{R}}$ is

$$t_{\mathbf{R}} = \frac{i(-1)^{R_x}}{\frac{L}{\pi}\sin(\frac{\pi R_x}{L})} \delta_{R_y,0} + \frac{(-1)^{R_y}}{\frac{L}{\pi}\sin(\frac{\pi R_y}{L})} \delta_{R_x,0}, \tag{3}$$

where the overall hopping amplitude has been set to unity. Note that Eq. (3) introduces electron hopping beyond nearest neighbors. We add a local repulsive Hubbard interaction,

$$H_U = U \sum_{\mathbf{i}} (n_{\mathbf{i}\uparrow} - 1/2)(n_{\mathbf{i}\downarrow} - 1/2), \tag{4}$$

where $U > 0$ is the interaction strength and $n_{\mathbf{i}\sigma} = c_{\mathbf{i}\sigma}^\dagger c_{\mathbf{i}\sigma}$ is the electron number operator. For sufficiently large U, we expect long-range Ising FM order in the z direction, which breaks time-reversal symmetry spontaneously and gaps out the Dirac cone. At half-filling, the single-particle density of states vanishes, thus we expect a line of finite-temperature transitions that terminates at a zero-temperature QCP with finite critical interaction strength U_c [22].

QMC method.—We employ a projector QMC (PQMC) method to analyze the quantum phase transition in our model system. In this method, the ground-state expectation value of an observable O is calculated using imaginary-time propagation of a trial wave function $|\Psi_T\rangle$ via $(\langle\Psi_0|O|\Psi_0\rangle/\langle\Psi_0|\Psi_0\rangle) = \lim_{\Theta\to\infty}(\langle\Psi_T|e^{-\Theta H} O e^{-\Theta H}|\Psi_T\rangle/\langle\Psi_T|e^{-2\Theta H}|\Psi_T\rangle)$. Here, we follow the approach introduced in Ref. [38] and choose an interacting trial wave function to further enhance the performance and convergence of the PQMC algorithm. We consider a Gutzwiller-projected wave function $|\Psi_T\rangle = e^{-g_{\mathrm{GW}} \sum_{\mathbf{i}} n_{\mathbf{i},\uparrow} n_{\mathbf{i},\downarrow}} |\mathrm{FS}\rangle$ which can be easily implemented as our trial state within QMC. Here, $|\mathrm{FS}\rangle$ is the noninteracting Fermi sea, and g_{GW} is the Gutzwiller variational parameter whose optimal value follows the approximate relation $g_{\mathrm{GW}} \approx 0.17U$. We perform calculations for system sizes $L \in \{5,7,9,11,13,15,17,19\}$, and use an imaginary projection time of $2\Theta = 14$ which is long enough to obtain ground-state properties. To demonstrate this, in Supplemental Material [32] we compare the performance of PQMC with a nontrivial Gutzwiller-projected state against regular PQMC ($g_{\mathrm{GW}} = 0$) as well as finite-temperature QMC. We find that the algorithm with $g_{\mathrm{GW}} \neq 0$ converges to the ground state the fastest. Moreover, an effective inverse temperature β_{eff} can be defined for a given projection time Θ such that the PQMC results are approximately equivalent to finite-temperature QMC results at temperature $T = 1/\beta_{\mathrm{eff}}$. We find that $\beta_{\mathrm{eff}}(g_{\mathrm{GW}} \neq 0) \approx 2\Theta + 11 \pm 1$ while $\beta_{\mathrm{eff}}(g_{\mathrm{GW}} = 0) \approx 2\Theta + 7 \pm 1$. Our PQMC method with $g_{\mathrm{GW}} \neq 0$ and $2\Theta = 14$ thus allows us to effectively reach temperatures as low as $\beta_{\mathrm{eff}} = 25 \pm 1$, which is sufficient to elucidate ground-state physics.

Although QMC is an unbiased method and is very effective for studying lattice models of strongly correlated electrons, its negative sign problem hinders its application to many problems of interest [39]. Nonetheless, the sign problem in QMC depends highly on the model's formulation, such that one may improve the energy scales that QMC can reach by choosing appropriately the Hubbard-Stratonovich (HS) decoupling of the interaction term. For the present model, the average sign is significantly higher if we decouple the interaction in the s_x or s_y channels rather than the usual s_z channel [Fig. 1(a)] [32]. With that decoupling, Fig. 1(b) shows that the average sign of our model at the QCP is not very severe, and we can reach sufficiently low temperatures to accurately predict ground-state properties.

FM transition.—We probe FM ordering in our model by computing the spin-spin correlation function,

$$M_{\mathbf{i}j} = \langle s_{z,\mathbf{i}} s_{z,\mathbf{j}} \rangle, \tag{5}$$

whose Fourier transform is the spin structure factor:

$$S(\mathbf{k}) = \frac{1}{L^4}\sum_{\mathbf{ij}} e^{i\mathbf{k}\cdot(\mathbf{i}-\mathbf{j})} M_{\mathbf{ij}}, \tag{6}$$

where $s_{z,\mathbf{i}} = \frac{1}{2}(n_{\mathbf{i}\uparrow} - n_{\mathbf{i}\downarrow})$ denotes the z component of the electron spin operator at site $\mathbf{i}$. In the broken-symmetry phase at large U, we expect long-range order at wave vector $\mathbf{k} = 0$ and the condensation of the $s_{z,\mathbf{i}}$ operator in the thermodynamic limit.

To explore the SM-to-FM QCP in QMC, we use two dimensionless quantities: the Binder ratio, defined here as

$$B \equiv \frac{\sum_{\mathbf{ijkl}} \langle s_{z,\mathbf{i}} s_{z,\mathbf{j}} s_{z,\mathbf{k}} s_{z,\mathbf{l}} \rangle}{(\sum_{\mathbf{ij}} \langle s_{z,\mathbf{i}} s_{z,\mathbf{j}} \rangle)^2}, \tag{7}$$

and the correlation ratio, defined as

$$R_{1,1} \equiv 1 - \frac{S(\mathbf{k} = \mathbf{k}^*)}{S(\mathbf{k} = 0)}, \tag{8}$$

where we define $\mathbf{k}^* \equiv (2\pi/L)(\hat{x} + \hat{y})$. Long-range FM ordering makes $S(\mathbf{k} = 0)$ diverge and hence implies $R_{1,1} \to 1$ in the thermodynamic limit $L \to \infty$. In the disordered SM phase, the correlation ratio vanishes in the thermodynamic limit since $S(\mathbf{k} \to 0) \to S(\mathbf{k} = 0)$. At the QCP, both B and $R_{1,1}$ are independent of L up to finite-size corrections. Therefore, we pinpoint the QCP by plotting these ratios as a function of U for various lattice sizes, and look for a crossing point of the curves. Using the Binder ratio, we identify the QCP to be $7.275 \leqslant U_c \leqslant 7.3$ [Fig. 2(a)]. The correlation ratio suggests the compatible result $7.25 \leqslant U_c \leqslant 7.275$ [Fig. 2(b)].

To further corroborate these results, we also measure the fermion excitation gap Δ_{SP} as a function of L and U using the unequal-time fermion Green's function [32]. In the thermodynamic limit, we expect $L\Delta_{\mathrm{SP}}(L \to \infty, U < U_c) \to 0$ in the gapless SM phase. Thus, we can estimate the position of the QCP by plotting $L\Delta_{\mathrm{SP}}(L, U)$ against $1/L$ and extrapolating to $L = \infty$ (see Fig. 3). This suggests $7.2 < U_c < 7.3$, consistent with the previous two approaches. These three methods combined indicate that $U_c \approx 7.275$. In Supplemental Material [32], we have computed B and $R_{1,1}$ using finite-temperature QMC with $\beta = L$ [25,40,41] for L up to 15 and achieve $7.25 < U_c < 7.3$, consistent with our PQMC results.

Critical exponents.—Having obtained a good estimate of U_c, we now turn to calculating universal critical exponents directly at the QCP. Those exponents describe the power-law decay of various correlation functions at the QCP. In Fig. 2(c), we plot the FM spin susceptibility, $S(\mathbf{k} = 0)$, for interaction strengths $U = 7.25$, 7.275, and 7.3. The spin susceptibility is expected to decay as $L^{-(1+\eta_\phi)}$ at the critical point for an $L \times L$ system. Figure 2(c) shows that the finite-size effects in the two-particle spin (bosonic) sector are insignificant as all data points follow a single straight line on a log-log scale. Our results in Fig. 2(c) thus suggest the anomalous dimension of the bosonic order parameter, η_ϕ, satisfies $0.282 < \eta_\phi < 0.352$. Likewise, the equal-time fermion single-particle Green's function in momentum space,

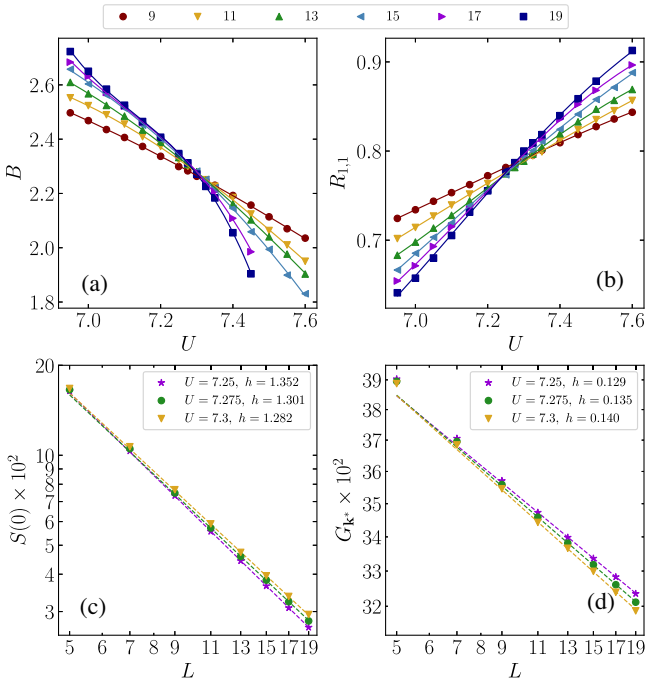

FIG. 2. (a) Binder ratio B and (b) correlation ratio $R_{1,1}$ as a function of U for various L (various symbols). The crossing point corresponds to U_c. We identify $7.25 < U_c \lesssim 7.3$ using these two methods. (c) FM spin susceptibility $S_{\mathbf{k}=0}$ and (d) equal-time fermion Green's function $G_{\mathbf{k}=\mathbf{k}^*}$ for various system sizes close to the critical point ($U = 7.25$, 7.275, 7.3). The observed linear behavior on a log-log scale is consistent with the expected power-law decay $S_{\mathbf{k}=0} \sim L^{-(1+\eta_\phi)}$ and $G_{\mathbf{k}=\mathbf{k}^*} \sim L^{-\eta_\psi}$ at criticality. The negative of the slope h is included for each U. We find $\eta_\phi = h - 1 \approx 0.31$ and $\eta_\psi = h \approx 0.135$ by taking the average across all three values of U.

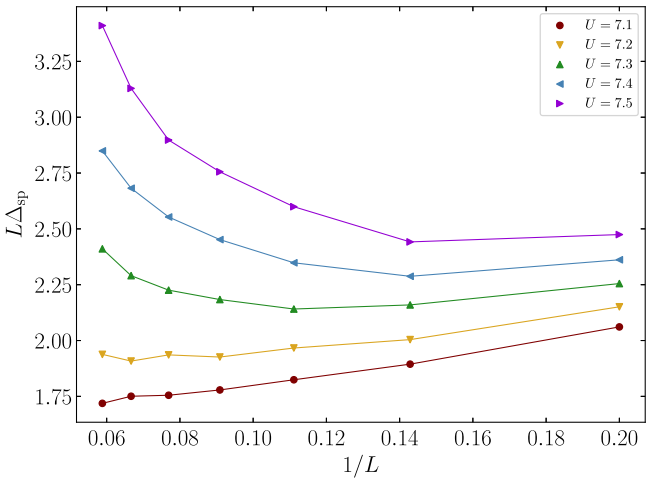

FIG. 3. Fermion single-particle gap Δ_{SP} as a function of $1/L$ for various values of U, which suggests $7.2 < U_c < 7.3$.

$G_{\mathbf{k}=\mathbf{k}^*}$, must decay as $L^{-\eta_\psi}$, where η_ψ is the anomalous dimension of the fermion operator at criticality. Accordingly, Fig. 2(d) shows that $0.129 < \eta_\psi < 0.140$. We obtained these numbers by taking the last five data points ($L = 11$, 13, 15, 17, 19) for fermions. We see that $L = 9$ follows the same line while $L = 5$, 7 exhibit visible deviations. This implies that finite-size effects are more pronounced in the fermionic sector. Among the three interaction strengths used in Figs. 2(c) and 2(d), our Binder : correlation ratio analysis suggests U_c is closer to 7.275. Thus, we conclude $\eta_\phi \approx 0.30 \pm 0.02$ and $\eta_\psi \approx 0.135 \pm 0.005$.

Alternatively, we can use the scaling hypothesis and data collapse near (but away from) the QCP to simultaneously obtain estimates of the critical exponents as well as U_c. Scaling forms for bosonic and fermionic correlation functions can be used to extract η_ϕ and η_ψ. We begin with the spin structure factor. At $\beta = \infty$ or $\beta = L$ and near the QCP, scaling analysis reveals that [42]:

$$L^{1+\eta_\phi} S_{\mathbf{k}=0}(L, U) = (1 + \alpha_1 L^{-\omega_1}) f_1(uL^{1/\nu}), \quad (9)$$

where $u = U - U_c$, ν is the correlation length exponent, and f_1 is a smooth scaling function of $uL^{1/\nu}$. The term proportional to $L^{-\omega_1}$ is an effective correction-to-scaling term which can be ignored for large systems. For $S_{\mathbf{k}=0}$ we find that those corrections are negligible and we achieve satisfactory results by keeping the leading scaling term. Such a simplified scaling hypothesis, namely $L^{1+\eta_\phi} S_{\mathbf{k}=0}(L, U) = f_1((U - U_c)L^{1/\nu})$, allows the following data-collapse method to extract the critical exponents. By plotting all available data points in the $L^{1+\eta_\phi} S_{\mathbf{k}=0}(L, U)$ combination against $(U - U_c)L^{1/\nu}$ and tuning U_c, ν, and η_ϕ to achieve a single smooth curve rather than scattered data points, we can identify both the critical exponents ν and η_ϕ and the critical point U_c [Fig. 4(a)]. This method yields $U_c \approx 7.280$, $\nu^{-1} \approx 1.19$, and $\eta_\phi \approx 0.310$. Again, finite-size effects are minimal here: we see in Fig. 4(a) that data points for systems as small as $L = 7$ also collapse to the fitting curve.

Additionally, near the QCP, the correlation ratio $R_{1,1}$ behaves as a universal function of $(U - U_c)L^{1/\nu}$ and L^z/β where z is the dynamical critical exponent and β the inverse temperature. Here, emergent Lorentz symmetry at the QCP implies $z = 1$. In Fig. 4(c), data collapse of $R_{1,1}$ yields the estimates $U_c \approx 7.265$ and $\nu^{-1} \approx 1.17$. We can also plot $L^{1+\eta_\phi} S(\mathbf{k} = 0)$ against $R_{1,1}$ to extract $\eta_\phi \approx 0.320$ [Fig. 4(b)]. The main advantage of this method compared to that used in Fig. 4(a) is that neither U_c nor ν need to be determined.

Similarly, to compute the fermion anomalous dimension η_ψ, we can utilize the following scaling hypothesis in the proximity of the QCP:

$$L^{\eta_\psi} G_{\mathbf{k}=\mathbf{k}^*}(L, U) = (1 + \alpha_2 L^{-\omega_2}) f_2(uL^{1/\nu}), \quad (10)$$

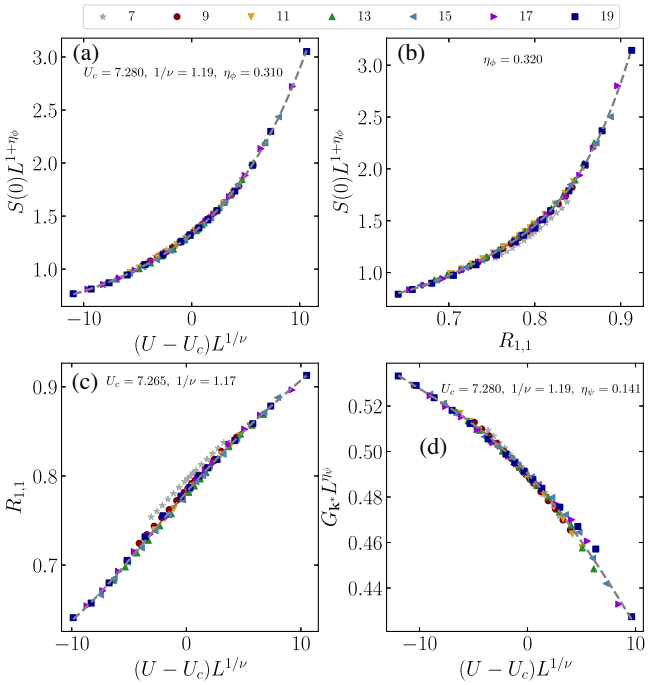

FIG. 4. Data collapse using the leading-order scaling hypothesis to estimate U_c and the critical exponents ν^{-1}, η_ϕ, and η_ψ. The numerical values of the estimated critical exponents are added to each sub-figure. The results are based on system sizes $9 \le L \le 19$, although we have plotted $L = 7$ using the estimated critical exponents as well.

where

$$G_{\mathbf{k}=\mathbf{k}^*}(L, U) \equiv \frac{1}{L^4} \sum_{\mathbf{ij}} e^{i\mathbf{k}^*\cdot(\mathbf{i}-\mathbf{j})} \langle c^\dagger_{\mathbf{i}\uparrow} c_{\mathbf{j}\downarrow} \rangle, \quad (11)$$

and f_2 is another smooth scaling function. Applying data collapse to $G_{\mathbf{k}^*}(L, U)$ yields satisfactory results, especially for $L \ge 9$ [Fig. 4(d)]. We find $\eta_\psi \approx 0.141$, $U_c \approx 7.280$, and $\nu^{-1} \approx 1.19$.

Combining our results directly obtained at the QCP and those extracted from data collapse in the vicinity of the QCP, we obtain a consistent set of critical exponent estimates with error bars that reflect the totality of our results (Table I). In Supplemental Material [32], we have investigated the impact of corrections to scaling on the critical exponents we extract. Although the quality of data collapse increases significantly upon introducing the associated free parameters $\alpha_{1,2}$ and $\omega_{1,2}$ in Eqs. (9) and (10), we find that the exponent values remain unchanged within the statistical error bar.

Summary and outlook.—In summary, we applied a PQMC method with Gutzwiller-projected trial state to study the quantum phase transition from paramagnetic Dirac semimetal to ferromagnetic insulator in a model of a single two-component Dirac fermion in $(2 + 1)D$ subject to an on-site repulsive Hubbard interaction U. We also performed finite-temperature QMC calculations for the

same model. Both methods yield consistent results, from which we conclude that the phase transition is continuous and happens at $U_c = 7.28 \pm 0.02$ in units of the fermion hopping amplitude. Besides determining the position of the QCP, our main result is a numerically exact determination of the critical exponents of the associated $N = 2$ chiral Ising GN universality class: the inverse correlation length exponent $\nu^{-1} = 1.19 \pm 0.03$, the order parameter anomalous dimension $\eta_\phi = 0.31 \pm 0.01$, and the fermion anomalous dimension $\eta_\psi = 0.136 \pm 0.005$.

The discrepancy between the conformal bootstrap and the other methods in Table I for ν^{-1} is more significant than for other critical exponents. Interestingly, this appears to be common to other Ising GN universality classes (see Table IV in Ref. [23]). For instance, for $N = 4$ Dirac flavors, the bootstrap predicts $\nu^{-1} \approx 0.76$ while a wide variety of QMC methods give answers in the range $1.06 \lesssim \nu^{-1} \lesssim 1.35$. For $N = 8$, the bootstrap predicts $\nu^{-1} \approx 0.88$ while QMC predicts $1.0 \lesssim \nu^{-1} \lesssim 1.3$. In both those cases, the previous QMC studies were sign-problem free and did not use SLAC fermions. This suggests the discrepancy for ν^{-1} in Table I is due neither to the use of SLAC fermions, the presence of a sign problem, nor the choice of QMC method. Our work adds to the growing number of QMC studies of Ising GN criticality that challenge the existing bootstrap estimates for ν^{-1}. Further and more accurate bootstrap studies of the GN universality classes are thus needed to resolve the discrepancy.

As a future direction, it would be interesting to apply the recently proposed adiabatic QMC algorithm [43] to our model Hamiltonian and study the robustness of our results at considerably lower temperatures. Additionally, our study can be extended to other values of N, in particular the $N = 1$ chiral Ising GN universality class which can be taken as an effective model of interacting Majorana surface states in the 3D topological superfluid ^{3}He-B [44,45]. Previous works on this universality class using the conformal bootstrap [17,46], FRG [18,47], and perturbative RG [14–16,48–50] have proposed that $\mathcal{N} = 1$ spacetime supersymmetry emerges at the $(2 + 1)D$ QCP. A numerical verification of this prediction would be of high value.

A. V. acknowledges useful discussions with Christian Mendl. S. M. T. and A. V. were supported by Iran Science Elites Federation (ISEF). J. M. was supported by NSERC Discovery Grants No. RGPIN-2020-06999 and No. RGPAS-2020-00064; the Canada Research Chair (CRC) Program; CIFAR; the Government of Alberta's Major Innovation Fund (MIF); the University of Alberta; the Tri-Agency New Frontiers in Research Fund (NFRF, Exploration Stream), and the Pacific Institute for the Mathematical Sciences (PIMS) Collaborative Research Group program. This research was enabled in part by support provided by Calcul Québec, Compute Ontario, WestGrid, and Compute Canada.

*Corresponding author.
vaezi@sharif.edu
†These two authors contributed equally.

[1] A. V. Balatsky, I. Vekhter, and J.-X. Zhu, Rev. Mod. Phys. **78**, 373 (2006).
[2] A. H. Castro Neto, F. Guinea, N. M. R. Peres, K. S. Novoselov, and A. K. Geim, Rev. Mod. Phys. **81**, 109 (2009).
[3] M. Z. Hasan and C. L. Kane, Rev. Mod. Phys. **82**, 3045 (2010).
[4] X.-L. Qi and S.-C. Zhang, Rev. Mod. Phys. **83**, 1057 (2011).
[5] X. Wan, A. M. Turner, A. Vishwanath, and S. Y. Savrasov, Phys. Rev. B **83**, 205101 (2011).
[6] T. Uehlinger, G. Jotzu, M. Messer, D. Greif, W. Hofstetter, U. Bissbort, and T. Esslinger, Phys. Rev. Lett. **111**, 185307 (2013).
[7] T. Wehling, A. Black-Schaffer, and A. Balatsky, Adv. Phys. **63**, 1 (2014).
[8] For a recent review of quantum critical phenomena in Dirac systems, see R. Boyack, H. Yerzhakov, and J. Maciejko, Eur. Phys. J. Special Topics **230**, 979 (2021).
[9] C. Xu, Phys. Rev. B **81**, 020411(R) (2010).
[10] T. Neupert, S. Rachel, R. Thomale, and M. Greiter, Phys. Rev. Lett. **115**, 017001 (2015).
[11] D. J. Gross and A. Neveu, Phys. Rev. D **10**, 3235 (1974).
[12] J. Zinn-Justin, Nucl. Phys. **B367**, 105 (1991).
[13] B. Rosenstein, H.-L. Yu, and A. Kovner, Phys. Lett. B **314**, 381 (1993).
[14] L. N. Mihaila, N. Zerf, B. Ihrig, I. F. Herbut, and M. M. Scherer, Phys. Rev. B **96**, 165133 (2017).
[15] N. Zerf, L. N. Mihaila, P. Marquard, I. F. Herbut, and M. M. Scherer, Phys. Rev. D **96**, 096010 (2017).
[16] B. Ihrig, L. N. Mihaila, and M. M. Scherer, Phys. Rev. B **98**, 125109 (2018).
[17] L. Iliesiu, F. Kos, D. Poland, S. S. Pufu, and D. Simmons-Duffin, J. High Energy Phys. 01 (2018) 036.
[18] G. P. Vacca and L. Zambelli, Phys. Rev. D **91**, 125003 (2015).
[19] Y.-T. Huang, L. Tsui, and D.-H. Lee, Nucl. Phys. **B954**, 115005 (2020).
[20] L. Wang, P. Corboz, and M. Troyer, New J. Phys. **16**, 103008 (2014).
[21] Z.-X. Li, Y.-F. Jiang, and H. Yao, New J. Phys. **17**, 085003 (2015).
[22] S. Hesselmann and S. Wessel, Phys. Rev. B **93**, 155157 (2016).
[23] E. Huffman and S. Chandrasekharan, Phys. Rev. D **101**, 074501 (2020).
[24] Y.-Y. He, X. Y. Xu, K. Sun, F. F. Assaad, Z. Y. Meng, and Z.-Y. Lu, Phys. Rev. B **97**, 081110(R) (2018).
[25] C. Chen, X. Y. Xu, Z. Y. Meng, and M. Hohenadler, Phys. Rev. Lett. **122**, 077601 (2019).
[26] Y.-X. Zhang, W.-T. Chiu, N. C. Costa, G. G. Batrouni, and R. T. Scalettar, Phys. Rev. Lett. **122**, 077602 (2019).
[27] Y. Liu, W. Wang, K. Sun, and Z. Y. Meng, Phys. Rev. B **101**, 064308 (2020).
[28] Y.-X. Zhang, H.-M. Guo, and R. T. Scalettar, Phys. Rev. B **101**, 205139 (2020).
[29] S. D. Drell, M. Weinstein, and S. Yankielowicz, Phys. Rev. D **14**, 1627 (1976).

[30] Z.-X. Li, A. Vaezi, C. B. Mendl, and H. Yao, Sci. Adv. **4**, eaau1463 (2018).
[31] T. C. Lang and A. M. Läuchli, Phys. Rev. Lett. **123**, 137602 (2019).
[32] See Supplemental Material at http://link.aps.org/supplemental/10.1103/PhysRevLett.128.225701 for more information, which includes Refs. [33–35].
[33] J. E. Hirsch, Phys. Rev. B **28**, 4059 (1983).
[34] J. E. Hirsch, Phys. Rev. B **29**, 4159(E) (1984).
[35] M. Feldbacher and F. F. Assaad, Phys. Rev. B **63**, 073105 (2001).
[36] By contrast, QMC simulations of chiral *XY* [30] or Heisenberg [31] quantum criticality with a single Dirac cone are sign-problem free.
[37] Furthermore, we chose the imaginary time step of $\Delta\tau = 0.05$ to keep the Trotter error well below our statistical error.
[38] M.-S. Vaezi and A. Vaezi, arXiv:1810.00864.
[39] M. Troyer and U.-J. Wiese, Phys. Rev. Lett. **94**, 170201 (2005).
[40] Y. Liu, Z. Wang, T. Sato, M. Hohenadler, C. Wang, W. Guo, and F. F. Assaad, Nat. Commun. **10**, 1 (2019).
[41] Z. H. Liu, M. Vojta, F. F. Assaad, and L. Janssen, Phys. Rev. Lett. **128**, 087201 (2022).
[42] Y. Otsuka, S. Yunoki, and S. Sorella, Phys. Rev. X **6**, 011029 (2016).
[43] M.-S. Vaezi, A.-R. Negari, A. Moharramipour, and A. Vaezi, Phys. Rev. Lett. **127**, 217003 (2021).
[44] T. Mizushima, M. Sato, and K. Machida, Phys. Rev. Lett. **109**, 165301 (2012).
[45] Y. J. Park, S. B. Chung, and J. Maciejko, Phys. Rev. B **91**, 054507 (2015).
[46] L. Iliesiu, F. Kos, D. Poland, S. S. Pufu, D. Simmons-Duffin, and R. Yacoby, J. High Energy Phys. 03 (2016) 120.
[47] H. Gies, T. Hellwig, A. Wipf, and O. Zanusso, J. High Energy Phys. 12 (2017) 132.
[48] H. Sonoda, Prog. Theor. Phys. **126**, 57 (2011).
[49] T. Grover, D. N. Sheng, and A. Vishwanath, Science **344**, 280 (2014).
[50] L. Fei, S. Giombi, I. R. Klebanov, and G. Tarnopolsky, Prog. Theor. Exp. Phys. **2016**, 12C105 (2016).